Autoionizing Rydberg series (np', nf') of Ar investigated by stepwise excitations with lasers and synchrotron radiation

Yin-Yu Lee, Tzan-Yi Dung, Re-Ming Hsieh, Jih-Young Yuh, Yen-Fang Song, Grace H. Ho, and Tzu-Ping Huang
National Synchrotron Radiation Research Center, Hsinchu Science Park, Hsinchu 30076, Taiwan

Wan-Chun Pan and I-Chia Chen
Department of Chemistry, National Tsing-Hua University, Hsinchu 30013, Taiwan

Shih-Yu Tu and A. H. Kung
Institute of Atomic and Molecular Sciences, Academia Sinica, Taipei, Taiwan Department of Photonics, National Chiao-Tung University, Hsinchu 30010, Taiwan

L. C. Lee
Department of Electrical and Computer Engineering, San Diego State University, San Diego, California 92182, USA
(Received 27 June 2008; published 12 August 2008)

Synchrotron radiation is used to excite Ar to the intermediate states $3p^5_{1/2}$ ($3d'[3/2]_1$, $5d'[3/2]_1$, $5s'[1/2]_1$, $7s'[1/2]_1$) and $3p^5_{3/2}$ ($6d[1/2]_1$, $6d[3/2]_1$, $8s[3/2]_1$), then excited by lasers to the autoionizing Rydberg series $3p^5_{1/2}\,np'$ ($[1/2]_{0,1}$, $[3/2]_{1,2}$) and $nf'[5/2]_2$. For the intermediate states of $5s'$, $7s'$, and $8s$, the np' ($[1/2]_0$ and $[3/2]_2$) series are observed with high intensity but not the np' ($[1/2]_1$ and $[3/2]_1$) series when the polarization vectors of two light beams are in parallel; but when they are in orthogonal, the $np'[1/2]_0$ series disappears, the $np'[3/2]_2$ intensity remains, and the np' ($[1/2]_1$ and $[3/2]_1$) series show up strongly. The intensity distribution of the np' series strongly depends on the intermediate state. The spectra of the np' series are assigned according to their intensity variation with the polarization vectors. The quantum defects determined for the series $np'[1/2]_0(n=11-57)$, $np'[3/2]_2(n=11-65)$, $np'[3/2]_1(n=11-31)$, and $nf'[5/2]_2(n=9-74)$ are 1.611 ± 0.011, 1.683 ± 0.013, 1.688 ± 0.010, and 0.016 ± 0.005, respectively. Our values are in excellent agreement with theoretical prediction. The spectral line shapes of autoionizing Rydberg states are analyzed with a Beutler-Fano profile. Reduced autoionization linewidths for the $np'[1/2]_0(n=11-16)$ series vary in the range 2549–4145 cm^{-1}, and the $nf'[5/2]_2(n=9-11)$ series in 186–247 cm^{-1} in reasonable agreement with theoretical prediction.

DOI: 10.1103/PhysRevA.78.022509 PACS number(s): 32.30.−r, 32.80.Rm, 32.80.Zb

I. INTRODUCTION

The odd-parity Rydberg series of Ar (ns, ns', nd, and nd') have been extensively investigated [1–3], but the even-parity series of np, np', nf, and nf' are not well known. The odd-parity series can be reached by optical excitation of Ar in the ground state $3p^6\,{}^1S_0$ but the even-parity series are optically forbidden by single-photon excitation so that they can be accessed only via the excited odd-parity Rydberg states. Because excited intermediate state atoms are difficult to prepare, to investigate the even Rydberg series is a challenging task. Stepwise excitation, preparing odd-parity Ar* atom by synchrotron radiation (SR) and then exciting it to an even-parity state by a laser, is an elegant way to do such a study. Here we report an extensive study on the even-parity autoionzing Rydberg series (ARS) with this technique.

In 1970, Yoshino [4] observed some weak even Rydberg series from excitation of Ar in the ground state, but these series are limited to the members below the first ionization threshold. High-energy members are hidden under strong absorption continua that resulted from direct photoionization of the Ar and Ar_2 dimer. Later, Dunning and Stebbings [5,6] observed some ARS between the first and second ionization thresholds ($9<n<26$) by ultraviolet excitation of metastable Ar $({}^3P_0)^*$ atoms generated from electron-impact excitation of Ar ($3p^6\,{}^1S_0$). They reported that every series member has only one single peak. In 1995, Koeckhoven *et al.* [7] observed some ARS in the same n range using four-photon excitation of Ar in the ground state. In their spectra, the $np'[1/2]_0$ and $np'[3/2]_2$ series were unresolved, in contrast to those of Kr and Xe that were well resolved. Based on observation of a single peak, Petrov *et al.* [8,9] assumed that the $np'[1/2]_0$ and $[3/2]_2$ states have the same resonance width in their calculation; their theorized linewidth turns out to differ from the experimental value by one order of magnitude. Further experimental measurements to test their calculation are clearly needed.

In 2005, Peters *et al.* [10] investigated the np' series by uv excitation of metastable Ar ($3p^5 4s^3P_2$) atoms produced by electrical discharge; they observed the $14p'$ member with a resolved structure. They expected that the $14p'$ member has three states: $[3/2]_2$, $[3/2]_1$, and $[1/2]_1$, but only two lines were barely resolved [10]. By comparing the observed absorption line shape with theoretical calculation, they assigned the observed broad line to $14p'$ $[1/2]_1$. Although the linewidth of $14p'$ $[1/2]_1$ agrees reasonably well, the linewidths of transitions to the $[3/2]_2$ and $[3/2]_1$ states are sharp in contrast to the calculated results. They attributed the disagreement to a lack of instrumental resolution. Better measurements of the linewidths and energies of these two states

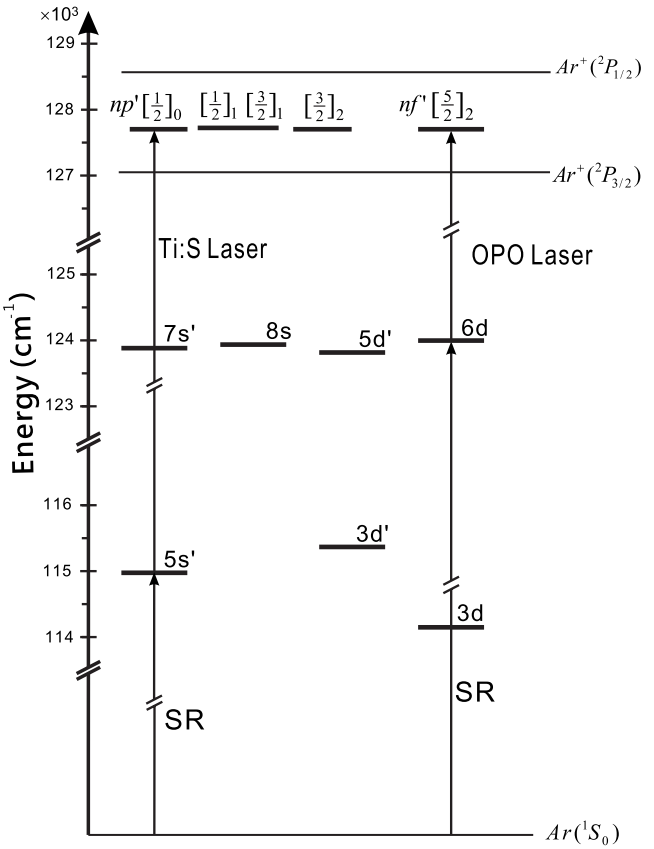

FIG. 1. Two-photon excitation scheme of Ar relevant to current investigation.

are needed to verify their theoretical calculations.

Recently, Petrov *et al.* [11] calculated the absorption cross sections to the four $14p'$ ($[3/2]_2$, $[3/2]_1$, $[1/2]_1$, and $[1/2]_0$) states by optical-excitation from an initial state, $3p^5 4s$ or $4s'$. They found that the absorption cross sections vary dramatically with the initial state; that is, the transition dipole moment strongly depends on the initial state. It is of interest to verify their calculation experimentally.

It is well established that stepwise-excitation experiments with a combination of SR and lasers provide an opportunity to obtain new scientific information [12–16]. SR has the advantage of ready accessibility and broad tunability in the high-energy photon region, and lasers have high intensity and high resolution. In a "pump-probe" experimental scheme, a SR beam serves to populate a selected and well-defined intermediate state that is subsequently examined with a laser beam. Using this technique, we can investigate various physical aspects of excited states that are forbidden to one-photon excitation by dipole selection rule.

All the states relevant to the current study are depicted in Fig. 1. The intermediate states are $3p^5_{1/2}$ ($3d'[3/2]_1$, $5d'[3/2]_1$, $5s'[1/2]_1$, $7s'[1/2]_1$) and $3p^5_{3/2}$ ($6d[1/2]_1$, $6d[3/2]_1$, $8s[3/2]_1$), and the ARS are $3p^5_{1/2}$ np' ($[1/2]_0$, $[1/2]_1$, $[3/2]_1$, $[3/2]_2$), and $nf'[5/2]_2$. Following the selection rules, the number of accessible states is limited; hence the ARS spectra are relatively simple and easy to analyze. We investigate the Rydberg series up to very high n members that are unreported.

II. EXPERIMENTAL

The experimental setup has been described elsewhere [16]. The experimental apparatus was comprised of two light sources and a vacuum chamber, containing a molecular beam source and a photoionization mass spectrometer [17], as shown in Fig. 2. A noble gas beam (400 Torr) was expanded through a nozzle (diameter 100 μm), skimmed into the interaction chamber and crossed with counterpropagating synchrotron radiation and laser beams in the ion-extraction region of a quadrupole mass filter (QMF) tuned at mass 40. The main chamber was typically operated at a pressure less than 3×10^{-7} Torr.

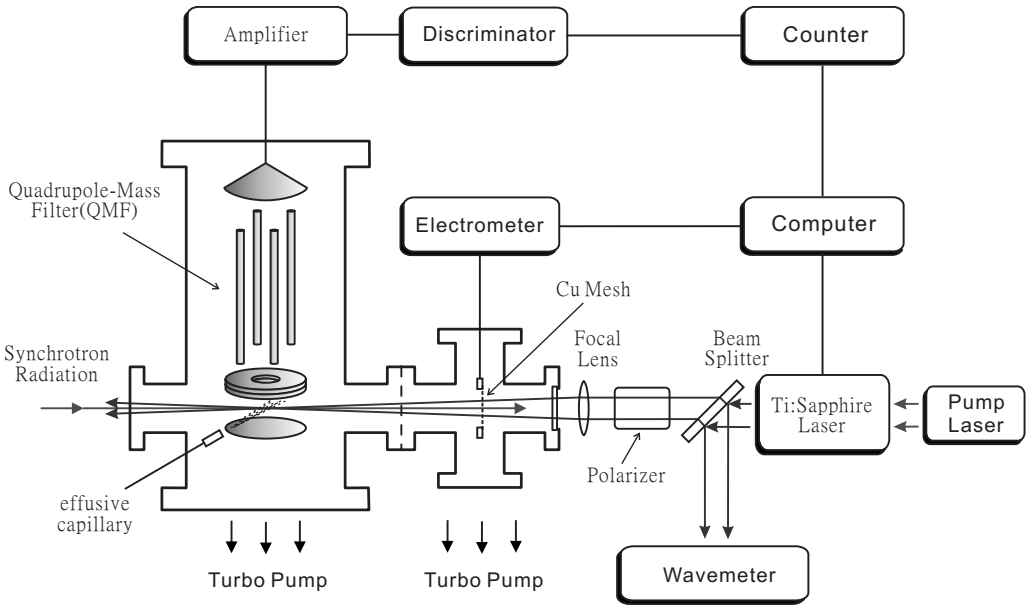

FIG. 2. Schematic experimental setup.

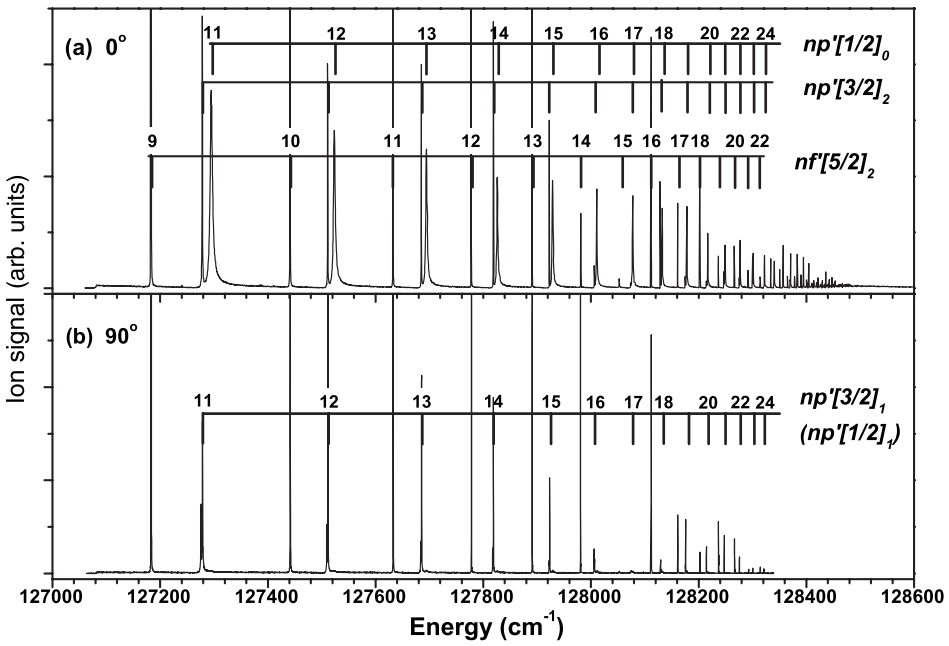

FIG. 3. Two-photon ionization spectra of Ar produced via the intermediate state $3p^5_{1/2}\ 5s'\ [1/2]_1$. The abscissa denotes a wavenumber sum of the Ti:sapphire laser and the intermediate state. The intensity is in arbitrary units. The polarization vectors of two light beams are (a) parallel, 0° and (b) perpendicular, 90°. The positions of the $3p^5_{1/2}\ np'$ ($[1/2]_0$ and $[3/2]_2$) and the $3p^5_{1/2}\ nf'$ $[5/2]_2$ states are indicated in (a), and the $3p^5_{1/2}\ np'$ ($[1/2]_1$ and $[3/2]_1$) states in (b).

The SR was provided by the high-resolution monochromatic beamline (BL21B2) equipped with cylindrical gratings that select photons in the energy range of 6–120 eV with resolving power of $E/\Delta E > 10^5$ [18]. The slit width was set at 50 μm that gave a resolving power $\sim 2\times 10^4$ at 15 eV, e.g., the resolution was about 6 cm^{-1}. Only a small fraction of light within the resonance line width of an intermediate state (in the order of 0.01 cm^{-1}) is absorbed. Near-infrared radiation was produced from a Ti:sapphire laser or an optical parametric oscillator (OPO) that propagated in a direction opposite to the SR and was mildly focused to a spot of diameter ~0.5 mm to match with the SR beam at the QMF ion-extraction region. The wavelength of the Ti:sapphire laser was measured by a wavemeter with an accuracy of 0.02 cm^{-1}. By rotating a birefringent filter with a computer-controlled linear actuator, the Ti:sapphire laser energy is tunable from 11690–13870 cm^{-1} (1.45–1.72 eV); its highest output power is 750 mW and its spectral width is ~0.25 cm^{-1}. The laser output is linearly polarized with an axial ratio greater than 300. The laser polarization is rotatable with a half-wave Fresnel rhomb polarizer. The laser was operated in the cw mode in this experiment.

For probing the high n members of ARS, a midinfrared OPO was implemented as the ionization source. The light source was a grazing-incidence periodically poled lithium niobate OPO similar to those described in previous reports [19,20]. This OPO laser is capable of producing more than one hundred milliwatts of infrared power in a bandwidth of 0.1 cm^{-1} in the 1.4–3 μm region. Continuous fine scanning was accomplished by rotating a mirror in the OPO cavity with a microstepping motor attached to a micrometer, controlled by a computer. The scanning range for the full width at half-maximum (FWHM) power at a single temperature and a crystal grating period was ~30 cm^{-1} [21]. Two concave gold-coated copper mirrors were used to focus the infrared beam into one of the two identical resonator tubes of a differential photoacoustic (PA) detector used for wavelength calibration of the OPO laser. The PA signal from H_2O or 200 ppmv of methane in nitrogen at 760 Torr and 25 °C [22] was measured with a phase-sensitive lock-in amplifier (SRS; Model 830) and recorded with a computer. The signal was plotted as a function of the motor step to obtain a PA spectrum. The spectrum was then displayed and calibrated with that of HITRAN [23] to provide the infrared (ir) wavelength.

III. RESULTS

A. Intermediate state $3p^5_{1/2}5s'[1/2]_1$

The photoionization spectrum produced via first excitation with SR to the intermediate state $3p^5_{1/2}5s'[1/2]_1$ at 114975.02 cm^{-1} [3] and then excited by a Ti:sapphire laser at varied photon energies is shown in Fig. 3. The abscissa denotes the wavenumber sum of the laser photon and the intermediate state. The intensity is in arbitrary units. In Fig. 3(a), the polarization vectors of two light beams are in parallel. The ARS positions for $3p^5_{1/2}$ ($np'\ [1/2]_0$, $np'\ [3/2]_2$ and $nf'[5/2]_2$) are indicated. For $n<16$, the peaks for every np' $[1/2]_0$ and $[3/2]_2$) pair is resolved; but at higher n, they are unresolved limited by the bandwidth of Ti:sapphire laser, but the structure is resolved using the OPO laser (see the spectra shown later). The intensities of the $np'\ [3/2]_2$ state are weaker than those of $np'\ [1/2]_0$ for $n=11$, 12, and 14, but they are reversed for $n=13$ and 15. The intensity of the nf' series is quite strong compared with those of the np'. When the angle, θ, between the polarization vectors of two light beams is rotated to 90°, the $np'\ [1/2]_0$ series disappears, but the np' ($[3/2]_1$ and $[1/2]_1$) series show up as shown in Fig. 3(b). The intensity of the $nf'[5/2]_2$ series is relatively intense compared with those of the np' ($[3/2]_1$ and $[1/2]_1$) series. The np' ($[3/2]_1$ and $[1/2]_1$) series are not optically allowed at $\theta=0°$, but they become allowed at $\theta=90°$. Since the nf' $[5/2]_2$ state is optically forbidden for transition from

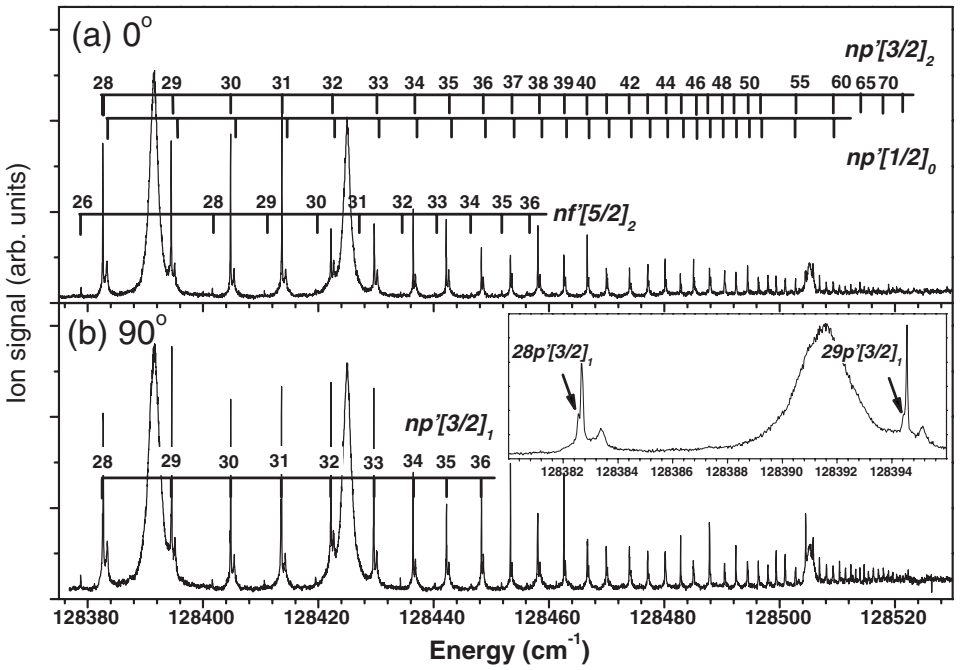

FIG. 4. Two-photon ionization spectra produced via the intermediate state $3p^5_{1/2}\ 7s'\ [1/2]_1$. The abscissa denotes a wavenumber sum of the OPO laser and the intermediate state. The polarization vectors of two light beams are (a) parallel and (b) perpendicular. The positions of the $3p^5_{1/2}\ np'$ ($[1/2]_0$ and $[3/2]_2$) and the $3p^5_{1/2}\ nf'$ $[5/2]_2$ states are indicated in (a), and the $3p^5_{1/2}\ np'\ [3/2]_1$ state in (b). The spectrum between 128380 and 128400 cm^{-1} is expanded in a panel in (b).

the intermediate state s' state but allowed from d and/or d' states, the intense nf' series shown in Fig. 3(b) may indicate that the $5s'$ state is mixed with d and/or d' character. The nf' series may also result from the Coulomb interaction between the Rydberg electron and the core electrons.

As shown in Fig. 3(a), the ion signal starts to appear at the total energy of 127078 cm^{-1} (15.7556 eV), which is about 32 cm^{-1} below the first ionization potential of Ar. Similar low thresholds for the Ar^+ appearance were reported by Koeckhoven *et al.* [7] and Radler and Berkowitz [24]; this is accounted for by the effect of electric field constantly applied in the QMF ion-extraction area. The electric field will induce collisional ionization of high-n Rydberg atoms below the ionization limit [7,24]. The dependence of the first Ar ionization potential on electric field has been systematically studied by Merkt [25] with a zero-kinetic-energy photoelectron-spectrum technology. Assuming that the first ionization potential of Ar is linearly dependent on electric field, the observed ion-signal threshold implies that the electric field in the QMF ion-extraction region is about 8 V/cm. This is consistent with the value estimated from the voltage applied in that region. The effect of electric field on the ARS of Ar is systematically investigated by Fielding and Softly [26]. Their results indicate that the electric field in our experiment is too low to disturb the angular momenta of the core and Rydberg electron as well as total angular momentum. At high electric field, for example, >100 V/cm, additional side-bands may appear nearby the ARS states [26], which do not show in our spectrum, indicating that our spectra are not distorted by the applied electric field.

B. Intermediate state $3p^5_{1/2}7s'[1/2]_1$

The spectrum produced via the state $3p^5_{1/2}7s'[1/2]_1$ of energy 123882.203 cm^{-1} [3] is shown in Fig. 4, where the OPO laser was used. For OPO laser experiments, there is no electric field in the QMF ion-extraction region during optical excitation period so that the spectra are free from possible electric field distortion. Figure 4(a) shows the spectrum observed at light-polarization vectors in parallel. The positions of the $3p^5_{1/2}np'[1/2]_0$ and $[3/2]_2$) states for $n=28-70$ and the $nf'[5/2]_2$ state for $n=26-36$ are indicated. The structure for the np' ($[1/2]_0$ and $[3/2]_2$) pair is well resolved, because the OPO laser has a high resolution. The intensity of the $[1/2]_0$ state is much weaker than that of $[3/2]_2$, differing from those shown in Fig. 3(a). The intensities of the $nf'[5/2]_2$ series are also relatively weak in comparison to that of np', implying that the $7s'$ state mixes little with the d and/or d' states, or the interaction between the Rydberg electron and the core electrons is weak.

When the polarization vectors were rotated to perpendicular, the spectrum varies significantly as shown in Fig. 4(b). There are two series appear at energy slightly below the $[3/2]_2$ as shown in the expanded inset of Fig. 4(b). These series are attributed to $np'\ [3/2]_1$ and $[1/2]_1$, which become optically allowed when the polarization vectors are orthogonal. It is noted that the intensity of the $np'\ [1/2]_0$ series is weak in both spectra of Fig. 4, when θ varies from 0 to 90°. This differs from the case of the $5s'[1/2]_1$ state where the intensity the $np'\ [1/2]_0$ series changes greatly as shown in the two spectra of Fig. 3.

As shown in Fig. 4, there are three additional bands at 128391.57, 128424.97, and 128505.20 cm^{-1}. These bands are quite broad when compared with the ARS bands. They may be produced by photodissociation of Ar_2^+ and/or Ar_2^* dimer excited in Rydberg states, a subject of further investigation in the near future.

C. Intermediate state $3p^5_{3/2}8s[3/2]_1$

The spectrum produced via the state $3p^5_{3/2}8s[3/2]_1$ at 123935.87 cm^{-1} [3] is shown in Fig. 5. The spectrum taken

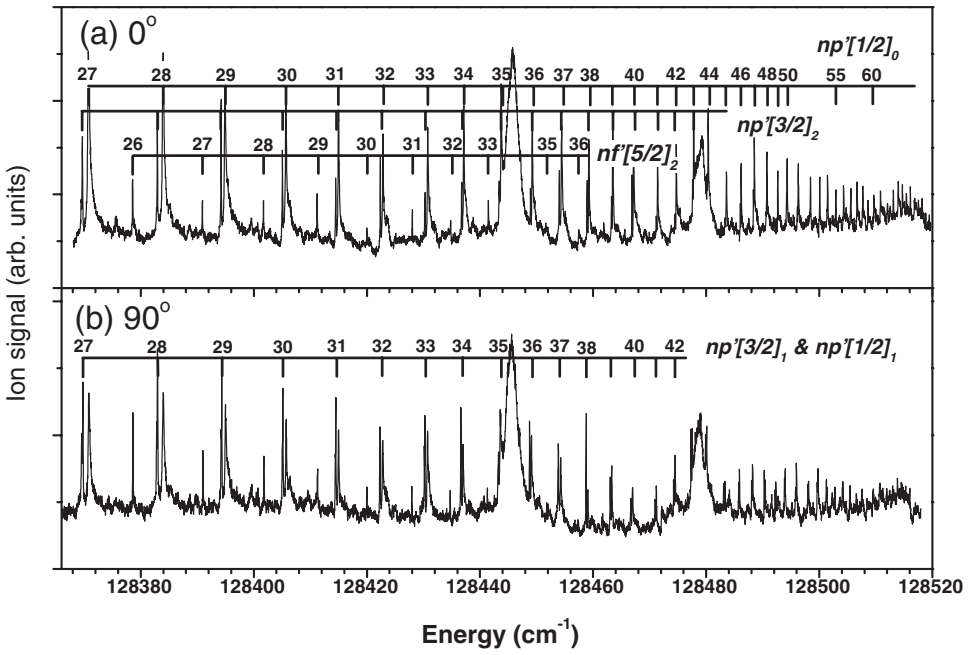

FIG. 5. Two-photon ionization spectra produced via the intermediate state $3p^5_{3/2}\,8s\,[3/2]_1$. The abscissa denotes a wavenumber sum of the OPO laser and the intermediate state. The polarization vectors of two light beams are (a) parallel and (b) perpendicular. The positions of the $3p^5_{1/2}\,np'$ ($[1/2]_0$ and $[3/2]_2$) and the $3p^5_{1/2}\,nf'$ $[5/2]_2$ states are indicated in (a), and the $3p^5_{1/2}\,np'$ ($[1/2]_1$ and $[3/2]_1$) states in (b).

with the polarization vectors of two light beams in parallel is shown in Fig. 5(a), where the OPO laser was used. The positions for the $3p^5_{1/2}\,np'$ ($[1/2]_0$ and $[3/2]_2$) and $nf'[5/2]_2$ states are indicated. In the spectrum, the intensity of the $[1/2]_0$ state is greater than that of $[3/2]_2$, in contrast to those of $5s'$ and $7s'$ shown in Figs. 3 and 4, respectively. The nf' series is quite strong when compared with np', indicating that the $8s$ state has a d and/or d' character, or the interaction between the Rydberg electron and the core electrons is strong.

When the polarization vectors are orthogonal, the intensity of the $[1/2]_0$ state deceases, but those of np' ($[3/2]_1$ and $[1/2]_1$) become intense as shown in Fig. 5(b). To find out the reason for such a dramatic variation of intensities is of interest and it is explainable by theoretical calculation that will be further discussed later. Again, two broad bands appear in the spectra at positions 128445.63 and 1284878.81 cm^{-1}, that may be from Ar_2^+ and/or Ar_2^*.

It is noted that the background signal shown in Fig. 5 is much stronger than those of $5s'$ and $7s'$ shown in Figs. 3 and 4, respectively. The larger background signal may be because of the intermediate state $3p^5_{3/2}8s[3/2]_1$ that has a core configuration similar to the first ionic state $Ar^+(^2P_{3/2})$, so that it can be more easily direct-photoionized into Ar^+ than the $3p^5_{1/2}ns'$ states that have a different ionic core.

D. Intermediate state $3p^5_{1/2}3d'[3/2]_1$

The $nf'[5/2]_2$ series appear up in the spectra shown in Figs. 3–5, which are attributed partly to the mixture of the s and s' states with the d and/or d' states; it is of interest to prove this possibility. The spectra produced via the $3p^5_{1/2}$ $3d'[3/2]_1$ state at 115366.866 cm^{-1} [3] combined with a Ti:sapphire laser are shown in Fig. 6. The spectrum taken with two polarization vectors in parallel is shown in Fig. 6(a), which is similar to the one shown in log scale in a previous

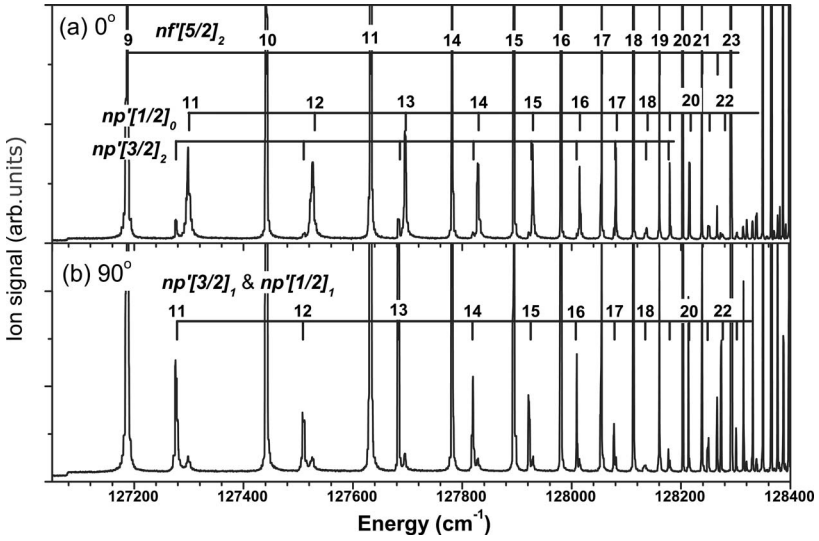

FIG. 6. Two-photon ionization spectra produced via the intermediate state $3p^5_{1/2}\,3d'\,[3/2]_1$. The abscissa denotes a wavenumber sum of the Ti:sapphire laser and the intermediate state. The polarization vectors of two light beams are (a) parallel and (b) perpendicular. The positions of the $3p^5_{1/2}$ np' ($[1/2]_0$ and $[3/2]_2$) and the $3p^5_{1/2}$ nf' $[5/2]_2$ states are indicated in (a), and the $3p^5_{1/2}$ np' ($[1/2]_1$ and $[3/2]_1$) states in (b).

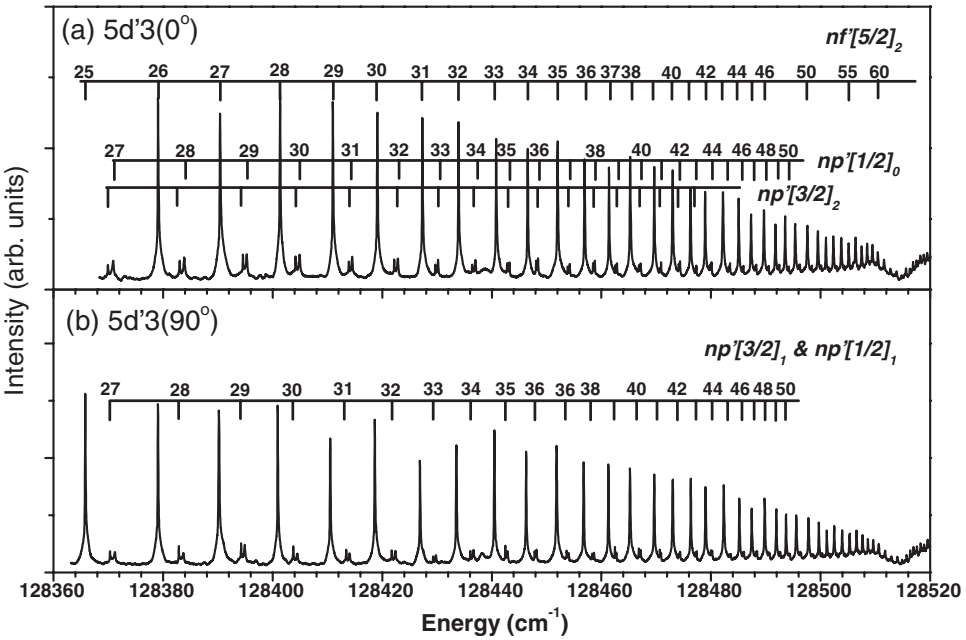

FIG. 7. Two-photon ionization spectra produced via the $3p^5_{1/2}\,5d'\,[3/2]_1$ intermediate state. The abscissa denotes a wavenumber sum of the OPO laser and the intermediate state. The polarization vectors of two light beams are (a) parallel and (b) perpendicular. The transitions to the $3p^5_{1/2}\,np'$ ($[1/2]_0$ and $[3/2]_2$) and the $3p^5_{1/2}\,nf'$ $[5/2]_2$ states are indicated in (a), and the $3p^5_{1/2}\,np'$ ($[1/2]_1$ and $[3/2]_1$) states in (b).

paper [16]. The positions of the $3p^5_{1/2}$ (np' $[1/2]_0$ and np' $[3/2]_2$) and $nf'[5/2]_2$ states for $n=9-23$ are indicated. The intensity of the nf' series is indeed about two orders of magnitude intense than those of np'. Although the np' series are optically allowed for transition from the intermediate state $3p^5_{1/2}3d'[3/2]_1$, their intensities are relatively weak. The larger intensity of the nf' series is explainable by the fact that its wave extends to a large distance from the core so that it has a better overlap with the Rydberg electron wave. It is noted that the intensity of $3p^5_{1/2}np'[1/2]_0$ is much intense than that of np' $[3/2]_2$.

The spectrum taken at the polarization vectors of two light beams in perpendicular is shown in Fig. 6(b). The intensity of the nf' series remains, but the intensity of np' $[1/2]_0$ is greatly reduced and the intensities of np' $[1/2]_1$ and $[3/2]_1$ increase.

E. Intermediate state $3p^5_{1/2}5d'[3/2]_1$

The spectra produced via the state $3p^5_{1/2}5d'[3/2]_1$ at 123815.56 cm^{-1} [3] combined with the OPO laser are shown in Fig. 7, where the polarization vectors of two light beams are (a) parallel and (b) perpendicular. The positions of the $3p^5_{1/2}$ (np' $[1/2]_0$ and np' $[3/2]_2$) and $nf'[5/2]_2$ states for $n=25-60$ are indicated in (a) and those of np' $[3/2]_1$ and $[1/2]_1$) for $n=27-50$ in (b). The intensity distributions of these two spectra are similar to that of the $3d'$ intermediate state as shown in Fig. 6, except the n members are much higher. These spectra are used to determine the quantum defects of high n members of the nf' series.

F. Intermediate state $3p^5_{3/2}6d$ ($[1/2]_1$ and $[3/2]_1$)

The spectra produced via $3p^5_{3/2}6d[1/2]_1$ at 123467.9733 cm^{-1} and $3p^5_{3/2}6d[3/2]_1$ at 123997.01 cm^{-1} states [3] combined with the OPO laser are shown in Fig. 8(a) for $n=28-58$ and in Fig. 8(b) for $n=45-70$, respectively, where the polarization vectors of two light beams are in parallel. The intensity distribution of these spectra are similar to those produced by other nd' states; the spectra are all dominated by the nf' series. However, it is noted that the continuum background signal produced by this $6d$ intermediate state is much higher than those of nd'. Again, this may be explainable by the fact that the $3p^5_{3/2}$ $6d$ state has the same core configuration as the first ionic state, $Ar^+(p^5_{3/2})$, so that it has an ir photoionization cross section greater than those of the $3p^5_{1/2}$ nd' states.

G. Dependence of intensity on θ

All the above spectra show that the relative intensities among the four np' series depend strongly on θ, the angle between the polarization vectors of two light beams. To further illustrate this effect, the spectra of the $11p'$ states produced via the $3p^5_{1/2}3d'[3/2]_1$ state at angles $\theta=0°$, 20°, 40°, 60°, 80°, and 90° are shown in Fig. 9. At $\theta=0°$, an intense line for the $11p'$ $[1/2]_0$ state appears at 127295.9 cm^{-1}, a weak line for $11p'$ $[3/2]_2$ at 127278.5 cm^{-1}, and a very weak line for $11p'$ $[3/2]_1$ at 127275.8 cm^{-1}. When θ increases, the intensity of the $[1/2]_0$ state decreases, and that of $[3/2]_1$ increases significantly; also, the $[1/2]_1$ state shows up as a broad feature with a peak position between the $[3/2]_1$ and $[3/2]_2$ lines. The intensity of the $[3/2]_1$ reaches maximum at θ near 90°, but the $[1/2]_0$ state systematically decreases to very small at $\theta=90°$. It is noted that the intensity for $[3/2]_2$ is independent of θ.

According to the j_cK-coupling principle that is generally applicable for rare gases and high n members, there are four states for an np' member, $3p^5_{1/2}np'$ ($[1/2]_0$, $[1/2]_1$, $[3/2]_1$, and $[3/2]_2$) [11,27,28] accessible from the current studied intermediate states. When $\theta=0°$, the np' ($[1/2]_0$ and $[3/2]_2$) states are optically allowed, but not np' $[1/2]_1$ and $[3/2]_1$. Transitions to these two $J=1$ states are optically forbidden because their transition moments contain a momentum factor

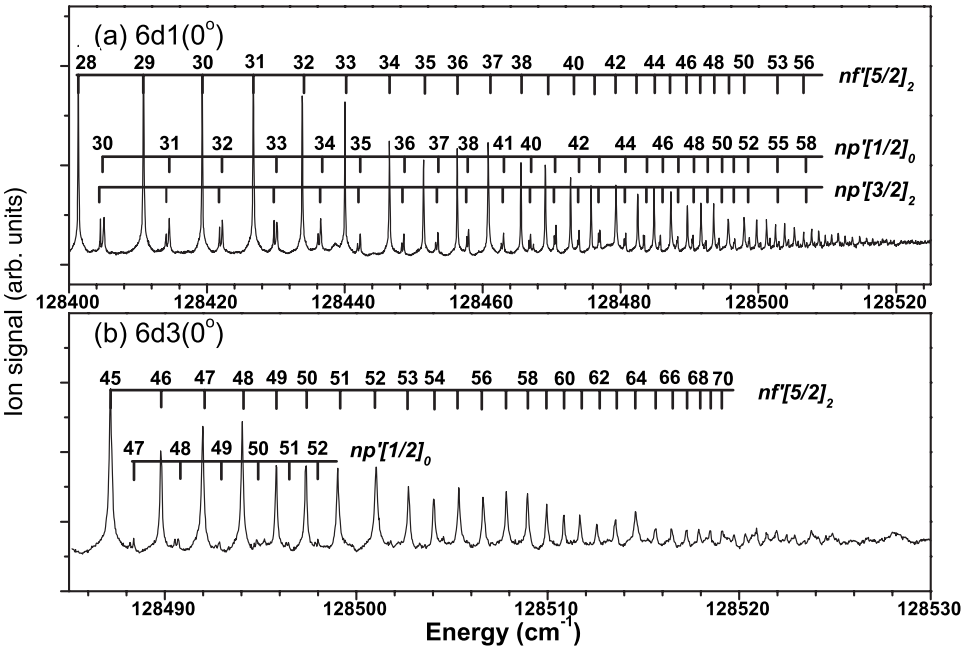

FIG. 8. Two-photon ionization spectra produced via the intermediate states (a) $3p^5_{1/2}\ 6d\ [1/2]_1$ and (b) $3p^5_{1/2}\ 6d\ [3/2]_1$, denoted as $6d1$ and $6d3$, respectively. The abscissa denotes a wavenumber sum of the OPO laser and the intermediate state. The polarization vectors of two light beams are in parallel. The transitions to the $3p^5_{1/2}\ np'$ ($[1/2]_0$ and $[3/2]_2$) and the $3p^5_{1/2}\ nf'\ [5/2]_2$ states are indicated in (a), and the $3p^5_{1/2}$ ($np'\ [1/2]_0$ and $nf'\ [5/2]_2$) states in (b).

that is equal to zero [28,29]. This selection rule is obeyed as shown in Fig. 9 at $\theta=0°$, where the intensity for the $J=1$ states is almost zero. When the polarization vectors of the light beams are orthogonal, the final states must have $M_J=\pm 1$ so that the $np'\ [1/2]_0$ state is not accessible [28]. In Fig. 9, when the polarization angles rotate from 0° to 90°, the intensity of the $[1/2]_0$ state deceases from a maximum to almost 0. (The small nonzero intensities for the $J=1$ states at $\theta=0°$ and the $J=0$ state at $\theta=90°$ may be caused by the imperfect light polarizations and/or the alignment between the light beams; the small nonzero intensities in turn show that the experimental condition is very good.) From the experimental spectra of Figs. 3–7 and 9, we conclude that the selection rules are generally followed.

IV. DISCUSSION

The experimental results show that the ARS spectra vary greatly with intermediate states and polarization angles. Based on selection rules and recent detailed theoretical calculations [8–11], our observed ARS positions can be assigned with great certainty. Also, our experiment provides autoionization-decay widths and quantum defects that can used to compare to calculations and thus to verify theory.

A. Assignment for the np' series

The photoabsorption cross section for the $4s'[1/2]_1 \rightarrow 14p'$ transition has been calculated by Petrov *et al.* [11] that is copied in Fig. 10(a) to compare with our observation

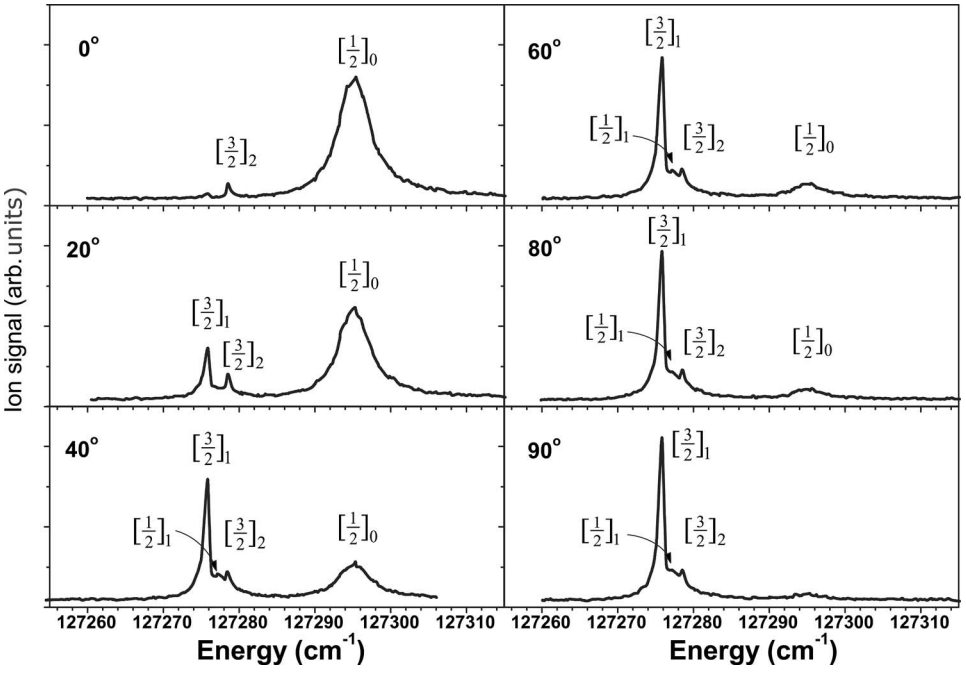

FIG. 9. Two-photon ionization spectra of $\mathrm{Ar}(3p^5_{1/2}\ 11p')$ produced via intermediate state $3p^5_{1/2}\ 3d'\ [3/2]_1$. The abscissa denotes a wavenumber sum of the Ti:sapphire laser and the intermediate state. The angles between the polarization vectors of two light beams vary from 0° to 90° as indicated. The positions of the $3p^5_{1/2}\ np'$ ($[1/2]_0$, $[1/2]_1$, $[3/2]_1$, and $[3/2]_2$) states are indicated.

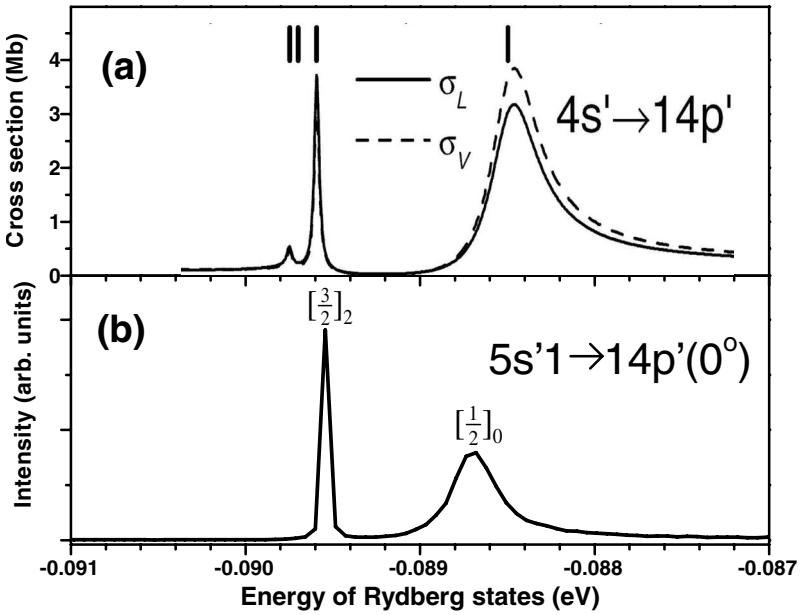

FIG. 10. (a) The spectrum calculated for the transitions $3p^5_{1/2}\ 4s'\ [1/2]_1 \rightarrow 3p^5_{1/2}\ 14p'$ ($[1/2]_0$, $[1/2]_1$, $[3/2]_1$, and $[3/2]_2$) (adopted from Fig. 3 in Ref. [11]). (b) Two-photon ionization spectrum of $Ar\{3p^5_{1/2}\ 14p'([1/2]_0$ and $[3/2]_2)\}$ produced via the intermediate state $3p^5_{1/2}\ 5s'\ [1/2]_1$, denoted as $5s'1$. The abscissa denotes the energy scale referred from the second ionization potential. The polarization vectors of two light beams are parallel.

on the $5s'[1/2]_1 \rightarrow 14p'$ transition at $\theta=0°$ in Fig. 10(b). Accordingly the broad line is assigned to the $14p'[1/2]_0$ state, the sharp one to $14p'[3/2]_2$, and the weak lines to $14p'$ ($[1/2]_1$ and $[3/2]_1$). The calculated position for the sharp line agrees well with the observed one, but the broad line has a larger calculated value of 0.2 meV ($\sim$1.6 cm^{-1}). The variation may be partly caused by different intermediate states ($4s'$ vs $5s'$). Absorption cross section depends on the transition dipole moment connecting the intermediate state to the np' states, it can thus be affected by intermediate state. The predicted weak line is not observed, but similar lines are observed in other spectra, for example, for $4s'[1/2]_1 \rightarrow 14p'$ in Fig. 10. In general, although there are some differences, the calculated and observed spectra do have a good agreement. The agreement implies that the assignment [11] for the positions of the np' series is reliable, which is adopted to analyze in all spectra observed.

As shown in Fig. 10, the observed band shape of $14p'[1/2]_0$ agrees well with theoretical calculation, but that of $14p'[3/2]_2$ is broader. The difference is likely caused by the large Ti:sapphire laser bandwidth of $\omega_{\text{laser}} \sim 0.25$ cm^{-1}. The actual line width can be obtained from the observed one by deconvolution over the laser bandwidth with an assumption of Gaussian line shape [1,2]

$$\omega^2_{\text{obs}} = \omega^2_{\text{line}} + \omega^2_{\text{laser}}. \quad (1)$$

From our observed width of $\omega_{\text{obs}}=0.71$ cm^{-1}, the actual linewidth is $\omega_{\text{line}}=0.66$ cm^{-1}, about twice larger than the calculated one [11].

B. Compare calculated cross section with measurement

The photoabsorption cross sections for the $4s'[1/2]_1$ and $4s[1/2]_1 \rightarrow 14p'$ transitions are computed by Petrov *et al.* [11] as copied in Figs. 11(a) and 11(b), respectively. They calculated the cross sections with (solid line) and without (dashed line) taking the virtual $4p$ shell into account. The spectra we select for comparison purposes are the $28p'$ states produced via two intermediate states $3p^5_{1/2}7s'[1/2]_1$ and $5p^5_{3/2}8s[3/2]_1$, which are shown in Figs. 4 and 5 and replotted in an expanded scale in Figs. 11(c) and 11(d), respectively. (It is noted that the n number is different from the theoretical one because of the availability of our data. At

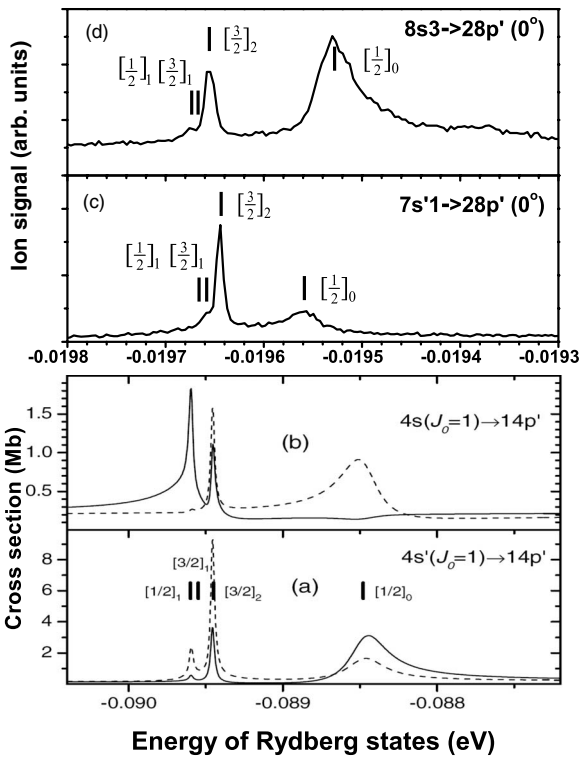

FIG. 11. The spectra calculated for the transitions (a) $4s'$ $(J_0=1) \rightarrow 14p'$ and (b) $4s$ $(J_0=1) \rightarrow 14p'$ (adopted from Fig. 4 in Ref. [11]). Two-photon ionization spectra of $Ar(3p^5_{1/2}\ 28p')$ produced via (c) the $3p^5_{1/2}\ 7s'\ [1/2]_1$ and (d) the $3p^5_{3/2}\ 8s\ [3/2]_1$, denoted as $7s'1$ and $8s3$, respectively. The abscissa denotes a wavenumber sum of the OPO laser and the intermediate states. The polarization vectors of two light beams are in parallel.

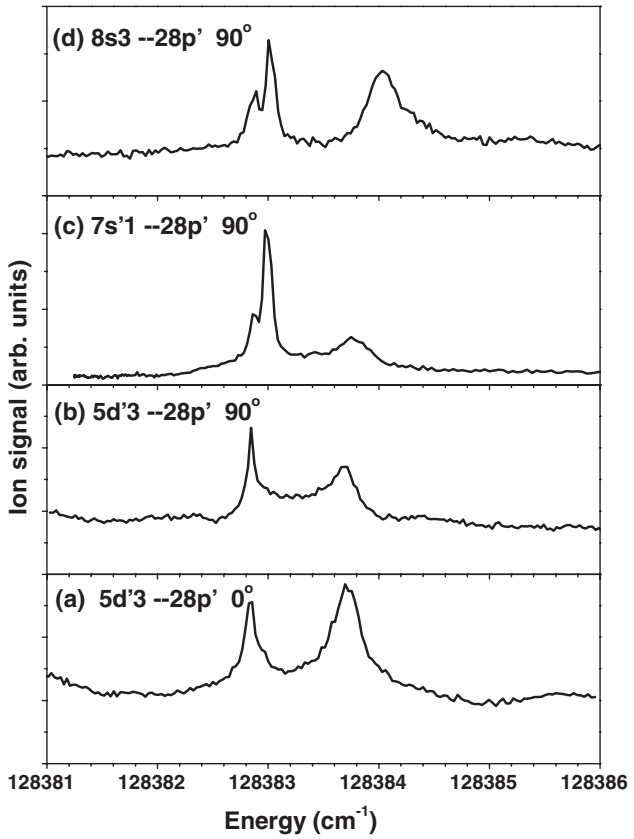

FIG. 12. Two-photon ionization spectra of Ar($3p^5_{1/2}$ $28p'$) produced via the intermediate state $3p^5_{1/2}$ $5d'$ $[3/2]_1$, denoted as $5d'3$ when the polarization vectors of two light beams are (a) parallel and (b) perpendicular. The spectra produced via (c) $3p^5_{1/2}$ $7s'$ $[1/2]_1$ and (d) $3p^5_{3/2}$ $8s$ $[3/2]_1$, denoted as $7s'1$ and $8s3$, respectively, are observed when the polarization vectors of two light beams are perpendicular.

different n numbers, the spectra will vary in detail, but their common shape and structure may be preserved. Therefore, although the comparison is not vital, it will provide a reasonable cross-check for theoretical calculation.) The calculated curves shown in Figs. 11(a) and 11(b) are compared with our spectra shown in Fig. 11(c) and 11(d), respectively. This comparison indicates that the calculation without taking the virtual $4p$ shell into account agrees better with our data. Especially, the large intensity of $[1/2]_0$ shown in Fig. 11(d) agrees with the dash line in Fig. 11(b), concluding that the calculation without taking the virtual shell into account is more favorable. Further theoretical calculations on the np' spectra are of interest.

C. Spectral dependence on intermediate state and polarization angle

The spectra of the np' series are affected by intermediate states and polarization angles as shown in Figs. 3–8. This effect is further illustrated in detail in Figs. 12(a)–12(d), where the $28p'$ spectra are produced via $5d'[3/2]_1$, $7s'[1/2]_1$, and $8s[3/2]_1$. Figures 12(a) and 12(b) show the spectra produced via $5d'[3/2]_1$ at $\theta=0°$ and 90°, respectively. As we know, the intensity of $[1/2]_0$, decreases when θ rotates from 0° to 90°, and the intensity of $[3/2]_2$ does not depend on θ. Comparing the spectra produced via $7s'$ and $8s$ at $\theta=90°$, as shown in Figs. 12(c) and 12(d), with those at $\theta=0°$ in Figs. 11(c) and 11(d), we find that the intensity ratio of the $[1/2]_0$ and $[3/2]_2$ states changes with θ. From these spectra observed, it is conclusive that although the np' spectra vary in detail, the common structures are generally preserved for varied intermediate states and polarization angles.

D. Confirm spectral assignment by polarization effect and linewidth

From the spectra in Figs. 9–12, it is clear that the ARS intensity distribution depends on the polarization angles, and the spectral intensity obeys selection rules. In summary, the $np'[1/2]_0$ has a maximum intensity at $\theta=0°$ and a minimum at 90°; the intensity of the $np'[3/2]_2$ is not affected by varying θ; and the intensities of both the np' ($[3/2]_1$ and $[1/2]_1$) series increase with increasing θ. This polarization effect can in turn be applied to confirm the assignment of the ARS states without ambiguity.

In addition to the polarization effect, the spectral assignment can also be cross-checked by comparing the calculated line width with the one observed. For instance, Petrov *et al.* [11] calculated that the linewidth of the $np'[1/2]_1$ state is about the same as that of $[1/2]_0$, but that of $[3/2]_1$ is about one order smaller. This confirms the assignment of the sharp peak at 12725.74 cm^{-1} shown in Fig. 9 to the $11p'[3/2]_1$ state and the broad band underneath to $11p'[1/2]_1$.

E. Spectral assignment of the nf' series

Based on the j_cK-coupling principle [22], a $3p^5_{1/2}nf'$ Rydberg member contains four states $[7/2]_4$, $[7/2]_3$, $[5/2]_3$, and $[5/2]_2$. With the intermediate states $3p^5_{1/2}$ ($3d'[3/2]_1$ and $5d'[3/2]_1$) and $3p^5_{3/2}$ $6d[3/2]_1$ studied in current experiment, only the $3p^5_{1/2}$ $nf'[5/2]_2$ series can be accessed by laser excitation. Since this series has only a single component, it is easy to identify as shown in Figs. 6–8. The $nf'[5/2]_2$ series is also produced via the $3p^5_{1/2}$ $5s'[1/2]_1$ intermediate state as shown in Fig. 3; this is likely caused by the mixture of $5s'$ with the nearby $3p^5_{1/2}$ $3d'[3/2]_1$ state, and/or a strong interaction between the Rydberg electron and the core electrons. The $nf'[5/2]_2$ series produced via the $3p^5_{1/2}$ $7s'[1/2]_1$ and $3p^5_{3/2}$ $8s[3/2]_1$ intermediate states are, however, quite weak as shown in Figs. 4 and 5, respectively.

Since the nf' state is single and well isolated, it is ideal for studying the dependence of intensity on polarization angle and intermediate state. As an example, the spectra of $9f'$ produced via the $3p^5_{1/2}$ $3d'[3/2]_1$ and $3p^5_{3/2}$ $3d[3/2]_1$ states are shown in Fig. 13. The line shapes produced via the $3d'$ state shown in Figs. 13(a) and 13(b) for $\theta=0°$ and 90°, respectively, are about the same; that is, the line shape does not depend on the polarization angle. In general, the line shapes of the nf' series produced via the $3d'$ and $5d'$ intermediate states are not affected by polarization angle.

The spectrum produced via the $3p^5_{3/2}$ $3d[3/2]_1$ intermediate state that was published in a previous paper [16] has a Beutler-Fano profile as shown in Fig. 13(c). This shape is

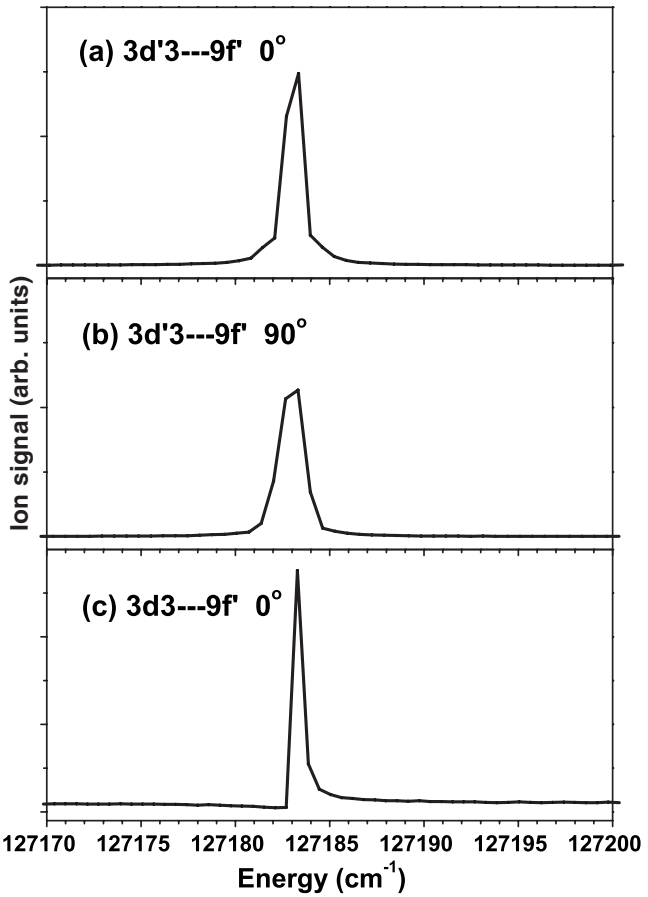

FIG. 13. Two-photon ionization spectra of $Ar(3p^5_{1/2}\,9f')$ produced via the intermediate state $3p^5_{1/2}\,3d'\,[3/2]_1$, denoted as $3d'3$, when the polarization vectors of two light beams are (a) parallel and (b) perpendicular. (c) The spectrum of $9f'$ produced via the intermediate state $3p^5_{3/2}\,3d\,[3/2]_1$, denoted as $3d3$, when the polarization vectors of two light beams are parallel.

quite different from all the other spectra presented in this paper. The profile is a result of an admixture between a discrete Rydberg state and an ionization continuum [30–32]. The profile implies that the $9f'$ state produced via the $3d$ state has a greater admixture with the continuum than that of $3d'$. This may in part due to the fact that the $3p^5_{3/2}\,3d[3/2]_1$ state has an ionic core same as the $Ar^+(3p^5p^2_{3/2})$ ion in the ground state so that it can be easily ionized by ir laser; this is evident by the high continuum background shown in Fig. 13(c). The line shapes will be further discussed later.

F. Quantum defect of the $np'[1/2]_0$ series

In accordance to the quantum defect theory [1,33], an ARS can be arranged into a Rydberg series by

$$E_{rn} = I_p - R_{\mathrm{Ar}}/(n-\mu_n)^2, \tag{2}$$

where E_{rn} and μ_n are the resonance energy and quantum defect for the n member of a Rydberg series, I_p is the ionization potential (IP) of the series, and R_{Ar} is the Rydberg constant for ^{40}Ar. All the ARS in our study are converging to the second limit $^{40}Ar^+(3p^5p^2_{1/2})+e^-$, for which the IP has been determined by many investigators [4,34–37]. Since our measurement covers to very high n numbers, the μ_n values are very sensitive to the IP value used. The latest IP values are 128541.425(4) cm^{-1} [36] and 128541.419(4) cm^{-1} [37] that are determined from the fine structure splitting of $^{40}Ar^+(^2P_{3/2}-{}^2P_{1/2})$ of 1431.5831 cm^{-1} [38] and the first ionization potential energy of 127109.842 cm^{-1} [36]. The average value of 128541.422 cm^{-1} is used for the μ_n calculation. The R_{Ar} value of 109735.809298 cm^{-1} was used in this calculation that was determined from recent atomic data [37–41].

When the line shape was analyzed with the Beutler-Fano profile, we found that the fitted resonance energy E_{rn} is slightly different from the energy at the peak position E_{pn}. At high n, they are close together so that they are not distinguishable. For the lowest n members we studied (i.e., $n=11$ for the np' series and 9 for nf'), the difference of μ_n values calculated by the resonance and peak energies is on the order of 10^{-3}, which has no affect for the accuracy offered here. Therefore, we simply use the measured peak energy for quantum defect calculation.

The energies for peak positions and quantum defects for the $np'[1/2]_0$ series are listed in Table I. The peak energies are taken from the $5s'$ intermediate state as shown in Fig. 3 for $n=11-29$, from $8s$ in Fig. 5 for $n=27-57$, and from $3d'$ in Fig. 6 for $n=11-33$. For the overlapped n region, the peak energy is averaged. The spectrum observed by Dunning and Stebbings [5,6] has unresolved structure of np' states, but it may be dominated by the $np'[1/2]_0$ series. Their peak energies agree with our measurements within 1 cm^{-1} for their highest members $n=24-26$, but there are generally lower for other members, for example, their values of 127269 or 127273 cm^{-1} for $n=11$ is lower than our value of 127294.88 cm^{-1} as listed in Table I.

The quantum defects are nearly constant for $n=9-30$, but they decrease about 2–5 % for $n=31-47$, and then slightly increase for the higher n members. The value averaged over all the $n=11-57$ members is 1.611 (11), where the number in parenthesis is one standard deviation. Our result agrees very well with the value of 1.614(8) for the $n=11-20$ members determined by Koeckhoven *et al.* [7] with a four-photon excitation of Ar in the ground state. It is noted that Koeckhoven *et al.* [7] mistakenly assigned their spectrum to $np'[3/2]_2$, but it shall be $np'[1/2]_0$ as pointed out by Peters *et al.* [10]. Our value over the same $n=11-20$ range is 1.617(2). This good agreement confirms the assignment made by Peters *et al.* [10].

Using a single-electron Pauli-Fock approach, Petrov *et al.* [8] calculated the quantum defects for the $15p'[1/2]_0$ and $20p'[1/2]_0$ states to be 1.565 and 1.564, respectively, which are about 3% lower than our value of 1.615 for both members. Including core polarization and electron correlation effect in the Pauli-Fock approach, Petrov *et al.* [11] recalculated a quantum defect to be 1.599 for the $n=14$ member, which is only about 1% below our value. The agreement between experiment and calculation is very good.

G. Quantum defect of the $np'[3/2]_2$ series

The peak energies and quantum defects for the $np'[3/2]_2$ series are listed in Table II. The peak energies are taken from

TABLE I. Peak positions E_p and quantum defects (QD) for the $np'\ [1/2]_0$ series.

n	E_p (cm^{-1})	QD	n	E_p (cm^{-1})	QD	n	E_p (cm^{-1})	QD
11	127394.88	1.617	27	128370.89	1.633	43	128477.59	1.538
12	127523.45	1.617	28	128383.63	1.629	44	128480.12	1.691
13	127694.70	1.616	29	128394.97	1.627	45	128483.37	1.522
14	127825.94	1.616	30	128405.32	1.606	46	128485.94	1.527
15	127928.92	1.615	31	128414.69	1.575	47	128488.25	1.571
16	128010.95	1.617	32	128422.68	1.600	48	128490.44	1.606
17	128077.61	1.618	33	128430.46	1.553	49	128492.35	1.711
18	128132.56	1.617	34	128437.08	1.570	50	128494.04	1.875
19	128178.08	1.621	35	128443.64	1.500	51	128496.00	1.848
20	128216.76	1.615	36	128448.83	1.574	52	128498.17	1.630
21	128249.06	1.626	37	128454.33	1.504	53	128499.82	1.641
22	128277.21	1.620	38	128459.12	1.485	54	128501.39	1.644
23	128301.35	1.620	39	128463.34	1.511	55	128502.84	1.669
24	128322.24	1.625	40	128467.04	1.590	56	128504.21	1.696
25	128340.62	1.623	41	128471.23	1.461	57	128505.50	1.729
26	128357.01	1.607	42	128474.54	1.494			
							average	1.611(11)

the $5s'$ intermediate state shown in Fig. 3 for $n=11-16$, from $7s'$ shown in Fig. 4 for $n=28-65$, and from $8s$ shown in Fig. 5 for $n=28-42$. The peak energy is an average value in the overlapped n region. The quantum defects are nearly constant up to $n=44$, and then fluctuate within 7% around the overall average value of 1.686(13). The quantum defect for $n=13$ and 14 measured by Peters *et al.* [10] with a single photon excitation from metastable Ar^* atom is 1.668(3), which is slightly lower than our value of 1.676(2) for the same n members. The theoretical value calculated [10] by Pauli-Fock approach is 1.628 for $n=15$. If core polarization and electron correlation effect is included, the value is 1.669

TABLE II. Peak positions E_p and quantum defects (QD) for the $np'\ [3/2]_2$ series.

n	E_p (cm^{-1})	QD	n	E_p (cm^{-1})	QD	n	E_p (cm^{-1})	QD
11	127278.47	1.679	36	128448.28	1.676	51	128496.30	1.685
12	127511.36	1.679	37	128453.32	1.709	52	128497.95	1.758
13	127685.45	1.677	38	128458.05	1.720	53	128499.37	1.916
14	127819.20	1.674	39	128462.60	1.688	54	128501.00	1.897
15	127923.26	1.676	40	128466.64	1.695	55	128502.76	1.724
16	128006.60	1.676	41	128469.94	1.820	56	128504.54	1.453
			42	128473.96	1.670	57	128505.78	1.513
28	128382.80	1.698	43	128477.13	1.686	58	128506.91	1.612
29	128394.52	1.669	44	128480.14	1.684	59	128508.09	1.622
30	128404.68	1.672	45	128482.77	1.745	60	128509.27	1.579
31	128413.72	1.686	46	128485.07	1.871	61	128510.37	1.553
32	128422.18	1.665	47	128487.82	1.754	62	128511.37	1.572
33	128429.64	1.669	48	128490.46	1.596	63	128512.34	1.573
34	128436.44	1.669	59	128492.41	1.682	64	128513.13	1.721
35	128442.31	1.726	50	128494.43	1.676	65	128513.93	1.821
							average	1.686(13)

TABLE III. Peak positionsE_p and quantum defects (QD) for the $np'\ [3/2]_1$ series.

n	E_p (cm^{-1})	QD	n	E_p (cm^{-1})	QD	n	E_p (cm^{-1})	QD
11	127275.74	1.689	16	128005.77	1.687	28	128382.88	1.691
12	127509.39	1.688	17	128073.40	1.688	29	128394.35	1.684
13	127683.90	1.688	18	128129.05	1.687	30	128404.80	1.660
14	127817.52	1.688				31	128413.96	1.659
15	127922.28	1.687	27	128369.61	1.728			
							average	1.688(10)

for $n=14$; it is later revised to 1.667 [11]. This theoretical value is only lower than our value by 0.4%, a remarkable good agreement.

H. Quantum defects of the np' ($[3/2]_1$ and $[1/2]_1$) series

The peak energies and quantum defects for the $np'[3/2]_1$ series are listed in Table III. The peak energies are taken from spectra observed with the polarization vectors of two light beams in orthogonal. The $7s'$, $8s$, and $3d'$ intermediate states provide the data for $n=28-31$, 27–31, and 11–18, respectively. The peak energy is an average value for an overlapped n member. The quantum defects are nearly constant for $n=11-18$, and they have a small fluctuation for large n members. The overall averaged value is 1.688(10). Muhlpfordt and Even [37] observed an ARS, likely due to the $np'[3/2]_1$ series, from optical excitation of Ar* in the $(3p^5_{1/2}\ 4s[3/2]_2)$ metastable state. Their quantum defect is 1.68(1), which is very close to our value. The theoretical value [10] calculated by Pauli-Fock approach is 1.636 for $n=15$, and it is 1.677 for $n=14$ including the core polarization and electron correlation effect [11]. These theoretical values are different from our experimental results by less than 1%; again, a remarkable good agreement.

The $np'[1/2]_1$ series is hidden underneath that of $np'[3/2]_1$ as shown in Fig. 9. It is difficult to determine the peak energies of this series accurately. However, these two lines are so close together that their peak energies shall be about the same; thus, their quantum defects will be similar too. This is consistent with the theoretical calculations that the quantum defects for these two states are almost identical [8–11]. In considering the good agreement between theoretical calculation and our experimental observation, it is believable that the calculated value is reliable.

I. Quantum defect of the nf' series

The observed nf' series has a very long progression as shown in Table IV. The peak energies are taken from the $3d'$ spectrum in Fig. 6 for $n=9-26$, from $5d'$ in Fig. 7 for $n=26-74$, and from $6d$ in Fig. 8 for $n=28-70$. The peak energy is an average value in the overlapped n region. The quantum defects are nearly constant for n up to 56, and gradually increase for the high n members. The overall averaged value is 0.016(5). Koeckhoven *et al.* [7] determined the value to be 0.010 (5) for $n=10-15$; Muhlpfordt and Even [42] gave a value of 0.072 (3) for $n=14-24$, compared to our value 0.005(3) averaged over $n=9-27$. Our result agrees better with the value from Koeckhoven *et al.* [7]. The theoretical value calculated by Pauli-Fock approach is 0.0005 for both $n=9$ and 20 [8–11]; and it is 0.00769 for $n=9$ if the core polarization and electron correlation effect is included in the Pauli-Fock approach [11]. Our value of 0.011 for $n=9$ agrees better with the latter calculation. Overall, our measurements again agree remarkable well with the theoretical calculations.

J. Autoionization width of the $np'[1/2]_0$ series

The ARS line shapes result from an admixture of discrete Rydberg states with ionization continua; they can be fitted by the Beutler-Fano profile [30–32]

$$I = I_0 + \Sigma_k I_k (q_k + \varepsilon_k)^2/(1+\varepsilon_k^2) \tag{3}$$

$$\varepsilon_k = 2(E - E_{rk})/\Gamma_k, \tag{4}$$

where I is the ion signal measured at energy E, I_0 is the background signal measured far away from the peak of a line, I_k, q_k, E_{rk}, and Γ_k are the ion signal, q parameter, resonance energy, and autoionization line width for a Rydberg state k, respectively.

As shown in Figs. 9–12, the $np'[1/2]_0$ series is well separated from nearby states so that it can be approximately treated as a single discrete state, and its shape can be fitted by the Beutler-Fano profile with $k=1$. Also, the observed width is much broader than the laser width; thus, the correction for the true linewidth with Eq. (1) is not needed. Instead of fitting the curve, a q parameter can be determined from the ratio of the half-intensity ($\mu_{1/2}$) and quarter-intensity ($\mu_{1/4}$) widths of the shape measured relative to the continuum background. The q parameter is determined by

$$q = [2(6a^2-1)/(1-3a^2)]^{1/2}, \tag{5}$$

where $a=\mu_{1/2}/\mu_{1/4}$. The autoionization line width is determined by

$$\Gamma = q\mu_{1/2}/(q^2+2)^{1/2}. \tag{6}$$

The resonance energy is determined from the energy at the peak E_p by

TABLE IV. Peak positions E_p and quantum defects (QD) for the $nf'\ [5/2]_2$ series.

n	E_p (cm^{-1})	QD	n	E_p (cm^{-1})	QD	n	E_p (cm^{-1})	QD
9	127183.30	0.011	31	128427.16	0.010	53	128502.33	0.018
10	127441.35	0.012	32	128434.15	0.016	54	128503.79	0.003
11	127632.70	0.011	33	128440.53	0.020	55	128505.12	0.023
12	127777.85	0.012	34	128446.49	0.001	56	128506.41	0.020
13	127890.90	0.012	35	128451.85	−0.001	57	128507.56	0.073
14	127980.72	0.010	36	128456.75	0.001	58	128508.72	0.077
15	128053.39	0.005	37	128461.25	0.003	59	128509.79	0.105
16	128112.30	0.009	38	128465.37	0.016	60	128510.83	0.108
17	128161.18	0.012	39	128469.19	0.020	61	128511.84	0.094
18	128202.26	0.013	40	128472.84	0.001	62	128512.79	0.097
19	128237.25	0.006	41	128476.03	0.035	63	128513.86	−0.098
20	128267.02	−0.002	42	128479.16	0.020	64	128514.60	0.043
21	128293.75	−0.007	43	128482.04	0.011	65	128515.50	−0.058
22	128314.84	−0.007	44	128484.84	−0.037	66	128516.27	−0.046
23	128334.17	−0.010	45	128487.23	0.001	67	128516.88	0.132
24	128350.91	0.000	46	128489.60	−0.018	68	128517.66	0.050
25	128365.79	0.004	47	128491.68	0.032	69	128518.33	0.064
26	128378.95	0.012	48	128493.73	0.035	70	128519.01	0.026
27	128390.99	−0.008	49	128495.69	0.015	71	128519.64	0.022
28	128401.81	0.017	50	128497.52	0.070	72	128520.30	−0.079
29	128410.81	0.014	51	128499.24	−0.005	73	128520.82	0.017
30	128419.48	0.002	52	128500.90	−0.041	74	128521.34	0.079
							average	0.016(5)

$$E_r = E_p - \Gamma/2q. \tag{7}$$

The energy at peak positions, half-widths, quarter-widths, q parameters, autoionization widths, reduced autoionization widths, and the differences of peak and resonance energies $\Delta E = E_p - E_r$ for the $np'[1/2]_0$ series produced via the $5s'$ intermediate states are listed in Table V. The reduced autoionization width is given by

$$\Gamma_r = n^{*3}\Gamma, \tag{8}$$

where $n^* = n - \mu_n$ is the effective principle quantum number. The data for the $11p'[1/2]_0$ state produced via $3d'[3/2]_1$ shown in Fig. 9 are also listed in Table V.

TABLE V. Peak positions E_p, full width at half-intensity $\mu_{1/2}$, full width at quarter-intensity $\mu_{1/4}$, width ratio $a = \mu_{1/2}/\mu_{1/4}$, q parameter, autoionization width Γ, effective quantum number n^*, reduced width Γ_r, and energy differences between peak and resonance ΔE for the $np'\ [1/2]_0$ series obtained via intermediate states $5s'\ [1/2]_1$ and $3d'\ [3/2]_1$.

n	E_p (cm^{-1})	$\mu_{1/2}$ (cm^{-1})	$\mu_{1/4}$ (cm^{-1})	a	q	Γ (cm^{-1})	n^*	Γ_r (cm^{-1})	ΔE (cm^{-1})
	$5s'\ [1/2]_1$								
11	127294.88	5.15	9.19	0.560	5.527	4.99	9.383	4122	0.45
12	127523.45	3.62	6.60	0.548	4.064	3.42	10.383	3827	0.42
13	127694.70	2.50	4.92	0.508	2.207	2.11	11.384	3106	0.48
14	127825.94	2.50	4.34	0.576	1.269	1.34	12.384	2549	0.53
15	127928.92	1.78	3.17	0.561	5.742	1.73	13.385	4145	0.15
16	128010.95	1.39	2.63	0.529	2.998	1.25	14.383	3715	0.22
	$3d'\ [3/2]_1$								
11	127294.88	4.95	8.66	0.572	9.838	4.90	9.383	4048	0.25

TABLE VI. Peak positions E_p, full width half-intensity $\mu_{1/2}$, full width at quarter-intensity $\mu_{1/4}$, width ratio $a=\mu_{1/2}/\mu_{1/4}$, q parameter, autoionization width Γ, effective quantum number n^*, reduced width Γ_r, and energy differences between peak and resonance ΔE for the $nf'[5/2]_2$ series obtained via intermediate states $3d'[3/2]_1$ and $3d[3/2]_1$.

n	E_p (cm^{-1})	$\mu_{1/2}$ (cm^{-1})	$\mu_{1/4}$ (cm^{-1})	a	q	Γ (cm^{-1})	n^*	Γ_r (cm^{-1})	ΔE (cm^{-1})
	$3d'[3/2]_1$ (no laser width correction)								
9	127183.30	0.57	1.03	0.553	4.54	0.54	8.989	395	0.06
10	127441.35	0.46	0.80	0.575	15.60	0.46	9.988	456	0.01
	$3d'[3/2]_1$ (corrected with laser width 0.25 cm^{-1})								
9		0.51	1.00	0.513	2.34	0.44	8.989	318	0.09
10		0.39	0.76	0.508	2.21	0.33	9.988	324	0.07
	$3d[3/2]_1$ (corrected with laser width 0.25 cm^{-1})								
9					3.11	0.34	8.989	247	
10					4.88	0.13	9.988	130	
11					4.83	0.14	10.989	186	

The difference between the peak and resonance energies shown in Table V is 0.45 cm^{-1} for $n=11$. The effective quantum defect calculated by this resonance energy of 127294.43 cm^{-1} is 1.619, which is only slightly smaller than the value of 1.617 calculated by the peak energy as listed in Table I. This justifies that the quantum defect can be calculated with peak energy without introducing significant error. It is worth noting that the line shapes are fitted very well by the Beutler-Fano profile with the q parameters determined by this method.

The reduced autoionization width is theoretically expected to be independent of the n number for a Rydberg series [1]. However, the Γ_r values in Table V show a large variation; especially, the value of 2549 cm^{-1} for the $n=14$ member is much smaller than that of 4145 cm^{-1} for $n=15$. The autoionization width results from the interaction between the discrete Rydberg state and ionization continuum [30]. The variation is mostly caused by the discrete state.

The averaged value of the reduced widths we measured at various n is 3644(250) cm^{-1}; this is comparable to the values of 4050(600) and 3780(360) cm^{-1} given by Koeckhoven *et al.* [7] and Petrov *et al.* [11], respectively. The theoretical values calculated by Pauli-Fock approach are 1783 cm^{-1} for $n=9$ and 1924 cm^{-1} for $n=20$ [8–11]; these values are much smaller than the experimental ones. When the core polarization and electron correlation effect is included in the Pauli-Fock approach, the calculated value is 3838 cm^{-1} for $n=9$ [11], which agrees reasonably well with experimental data. These results indicate that the reduced width is a more sensitive way than the level energy to test theory.

K. Autoionization widths of the np' ($[1/2]_1$ and $[3/2]_1$) series

The $np'[1/2]_1$ and $[3/2]_1$ series observed at orthogonal polarization vectors are overlapped together and mixed with the $[3/2]_2$ series as well. To get the widths and resonance energies, it requires fit the line profile with three channels in Eq. (3). The fitting procedure is cumbersome, and the obtained parameters are much less accurate. For the $11p'[3/2]_2$ state shown in Fig. 9, its intensity is weak and does not depend on the polarization angle so that it can be easily subtracted out from the spectra. Also, the $11p'[3/2]_1$ state is sharp and intense, it can be separated from the $11p'[1/2]_1$ state that is broad and weak. The autoionization widths determined from the $11p'$ ($[1/2]_1$ and $[3/2]_1$) states shown in Fig. 9 are about 3.6 and 0.4 cm^{-1}, respectively. This is consistent with the calculation by Petrov *et al.* [11] that the linewidth of the $np'[1/2]_1$ state is about the same as that of $np'[1/2]_0$, but it is about one order larger than that of $np'[3/2]_1$.

L. Linewidth of the $nf'[5/2]_2$ series

As shown in Figs. 6–8, the $nf'[5/2]_2$ series is well isolated from other states; thus, its linewidth can be determined by Eqs. (3)–(8) with the width ratios measured. The results for $9f'$ and $10f'$ produced via $3p_{1/2}^5\,3d'[3/2]_1$ shown in Fig. 6 are listed in Table VI. It shows that the half-width is only about twice that of the laser width ~0.25 cm^{-1}; therefore, a correction on the observed width to get the true linewidth by Eq. (1) is needed. After the correction of laser width, the reduced autoionization widths are 318 and 324 cm^{-1} for $n=9$ and 10, which are smaller than the uncorrected values of 395 and 456 cm^{-1}, respectively. Petrov *et al.* [11] calculated the reduced width for the $n=9$ state to be 185.7 cm^{-1} using the Pauli-Fock approach, and decreases to 181.8 cm^{-1} if configuration interaction and core polarization are included in calculation. Our value is higher than the calculated one by a factor of about 2; this difference is mainly caused by the laser resolution not good enough to measure the linewidth accurately.

The line shape produced via the intermediate state $3p_{1/2}^5\,3d[3/2]_1$ shown in Fig. 13(c) is another type of Beutler-Fano profile that can also be fitted by Eq. (3) with a q parameter determined by

$$q=[(I_p-I_c)/(I_c-I_m)]^{1/2}, \tag{9}$$

where I_p, I_c, and I_m are the intensity at the peak, continuum, and minimum, respectively.

The autoionization width is determined by

$$\Gamma = 0.5q(E_p - E_m)/(q^2+1), \quad (10)$$

where E_p and E_m are the energies at the peak and minimum, respectively.

The q parameters, autoionization widths, and reduced autoionization widths for $9f'$, $10f'$, $10f'$, and $11f'$ produced by the $3d\ [3/2]_1$ intermediate state (also, see the spectrum published in our previous paper [16]) are listed in Table VI. In this analysis, the q parameter is determined by relative intensities, and the autoionization width is determined by relative energies at the maximum and minimum intensities so that it is less affected by the laser width. The averaged Γ_r value for $n=9-11$ as shown Table VI is 188 cm^{-1}, which is in excellent agreement with the theoretical value of 181.8 cm^{-1} [11].

M. Photodissociation of the Ar_2^+ ion

Three broad bands are observed in the spectrum with peaks at 128391.57, 128424.97, and 128505.20 cm^{-1} in Fig. 4; two bands with peaks at 128445.63 and 128478.81 cm^{-1} in Fig. 5; and one weak band at 128438.50 cm^{-1} in Fig. 7. These bands are much broader than an atomic line. The $^{40}Ar^+$ signals observed at these bands are likely produced from photodissociation of Ar_2^+ ion and/or Ar_2^* dimer excited in Rydberg states. Radler and Berkowitz [24] have observed the Ar_2^+ ion long ago when Ar atoms in the ground state were excited to the $7s'$ and $8s$ states. Photodissociation of Ar_2^+ in the ground state to produce Ar^+ was studied long time ago by Lee *et al.* [43] and Moseley *et al.* [44]. They have observed an absorption band in the range from 11900 to 15630cm^{-1}. This absorption band does not fit our current observation. Further study on this subject is of interest.

V. CONCLUDING REMARKS

Ar atoms in the ground state are excited by synchrotron radiation to the intermediate states $3p^5_{1/2}$ ($3d'\ [3/2]_1$, $5d'\ [3/2]_1$, $5s'\ [1/2]_1$, $7s'\ [1/2]_1$) and $3p^5_{3/2}$ ($6d\ [1/2]_1$, $6d\ [3/2]_1$, $8s\ [3/2]_1$), and then excited by lasers to the autoionizing Rydberg series $3p^5_{1/2}\ np'$ ($[1/2]_0$, $[1/2]_1$, $[3/2]_1$, $[3/2]_2$) and $nf'\ [5/2]_2$. When the polarization vectors of two light beams are in parallel, one-photon excitation of the intermediate states $5s'$, $7s'$, and $8s$, produces intense np' ($[1/2]_0$ and $[3/2]_2$) series but not the np' ($[1/2]_1$ and $[3/2]_1$) series. When the polarization vectors are in orthogonal, the $np'\ [1/2]_0$ series disappears and the np' ($[1/2]_1$ and $[3/2]_1$) series show up strongly. The spectral intensity depends on the angle between the polarization vectors of two light beams in accord with selection rules. This polarization effect is a powerful tool to identify Rydberg states. This technique can be extended to study the spectral properties of other rare gases and further to molecules.

The intensity distribution of the np' series strongly depends on intermediate state. The intensity ratios of the two np' ($[1/2]_0$ and $[3/2]_2$) series vary dramatically with the intermediate states $5s'$, $7s'$, and $8s$ and the n number as well. For the intermediate states $3d'$, $5d'$, and $6d$, the intensity of the $nf'\ [5/2]_2$ series is about two orders of magnitude stronger than those of np'. Such large variation is mostly related to the nature of the intermediate state. This result implies that this stepwise technique can be applied to study the nature of Rydberg states.

The spectrum produced by stepwise optical excitation is simple and easy to analyze so that each ARS is observed up to the n numbers much higher than published ones. Since a large number of a Rydberg series are observed, the quantum defects calculated will be more accurate. To extend the current study to other rare-gas atoms and possibly to molecules is of interest.

ACKNOWLEDGMENTS

We thank Yuan-Pern Lee at National Chao-Tong University in Taiwan for a critical review and valuable comments. We also thank Gloria Fountain for her suggestions and comments. L. C. Lee and W.-C. Pan thank the National Synchrotron Radiation Research Center (NSRRC) in Taiwan. The National Science Council in Taiwan and Academia Sinica, Taipei provided the financial support.

[1] J. Berkowitz, *Photoabsorption, Photoionization, and Photoelectron Spectroscopy* (Academic Press, New York, 1979).
[2] J. Berkowitz, Adv. Chem. Phys. **72**, 1 (1988).
[3] Yu. Ralchenko, A. E. Kramida, J. Reader, E. B. Saloman, J. J. Curry, D. E. Kelleher, J. R. Fuhr, L. Podobedova, W. L. Wiese, K. Olsen, G. R. Delton, R. Dragoset, F. C. Jou, W. C. Martin, P. J. Mohr, A. Musgrove, C. J. Sansonetti, and G. Wiersma, *NIST Atomic Spectra Database* (version 3.1.5), http://physics.nist.gov/asd3
[4] K. Yoshino, J. Opt. Soc. Am. **60**, 1220 (1970).
[5] R. F. Stebbings and F. B. Dunning, Phys. Rev. A **8**, 665 (1973).
[6] F. B. Dunning and R. F. Stebbings, Phys. Rev. A **9**, 2378 (1974).
[7] S. M. Koeckhoven, W. J. Buma, and C. A. de Lange, Phys. Rev. A **51**, 1097 (1995).
[8] I. D. Petrov, V. L. Sukhorukov, and H. Hotop, J. Phys. B **35**, 323 (2002).
[9] I. D. Petrov, V. L. Sukhorukov, and H. Hotop, J. Phys. B **36**, 119 (2003).
[10] T. Peters, T. Halfmann, U. Even, A. Wünnenberg, I. D. Petrov, V. L. Sukhorukov, and H. Hotop, J. Phys. B **38**, S51 (2005).
[11] I. D. Petrov, T. Peters, T. Halfmann, S. Aloïsc, P. O'Keeffe, M. Meyer, V. L. Sukhorukov, and H. Hotop, Eur. Phys. J.: Appl. Phys. **40**, 181 (2006).
[12] M. Gisselbrecht, A. Marquette, and M. Meyer, J. Phys. B **31**, L977 (1998).
[13] M. Meyer, M. Gisselbrecht, A. Marquette, C. Delisle, M. Larzillière, I. D. Petrov, N. V. Demekhina, and V. L. Sukhorukov, J. Phys. B **38**, 285 (2005).

[14] S. Aloïse, P. O'Keeffe, D. Cubaynes, M. Meyer, and A. N. Grum-Grzhimailo, Phys. Rev. Lett. **94**, 223002 (2005).
[15] X. Qian, T. Zhang, C. Y. Ng, A. H. Kung, and M. Ahmed, Rev. Sci. Instrum. **74**, 2784 (2003).
[16] Y.-Y. Lee, T.-Y. Dung, J.-Y. Yu, Y.-F. Song, K.-T. Hsu, and K.-K. Lin, J. Electron Spectrosc. Relat. Phenom. **144-147**, 29 (2005).
[17] G. H. Ho, M. S. Lin, Y. L. Wang, and T. W. Chang, J. Chem. Phys. **109**, 5868 (1998).
[18] Y. F. Song, J.-Y. Yuh, Y.-Y. Lee, S. C. Chung, L. R. Huang, K.-D. Tsuei, S. Y. Perng, T. F. Lin, H. S. Fung, C.-I. Ma, C. T. Chen, and K. L. Tsang, Rev. Sci. Instrum. **77**, 085102 (2006).
[19] F. Kühnemann, K. Schneider, A. Hecker, A. A. E. Martis, W. Urban, S. Schiller, and J. Mlynek, Appl. Phys. B **66**, 741 (1998).
[20] C.-S. Yu and A. H. Kung, J. Opt. Soc. Am. B **16**, 2233 (1999).
[21] A. Miklós, C.-H. Lim, W.-W. Hsiang, G.-C. Liang, A. H. Kung, A. Schmohl, and P. Hess, Appl. Opt. **41**, 2985 (2002).
[22] G.-C. Liang, H.-H. Liu, A. H. Kung, A. Mohacsi, A. Miklos, and P. Hess, J. Phys. Chem. A **104**, 10179 (2000).
[23] HITRAN2004(v12.0) database, http://www.cfa.harvard.edu/hitran/
[24] K. Radler and J. Berkowitz, J. Chem. Phys. **70**, 221 (1979).
[25] F. Merkt, J. Chem. Phys. **100**, 2623 (1994).
[26] H. H. Fielding and T. P. Softley, J. Phys. B **25**, 4125 (1992).
[27] R. D. Cowen, *The Theory of Atomic Structure and Spectra* (University of California Press, Berkeley, CA, 1981).
[28] I. D. Petrov, V. L. Sukhorukov, T. Peters, O. Zehnder, H. J. Wörner, F. Merkt, and H. Hotop, J. Phys. B **39**, 3159 (2006).
[29] R. N. Zare, *Angular Momentum: Understanding Spatial Aspects in Chemistry and Physics, The George Fisher Baker Non-Resident Lectureship in Chemistry at Cornell University*, 1st ed. (Wiley, New York, 1988).
[30] U. Fano, Phys. Rev. **124**, 1866 (1961).
[31] U. Fano and J. W. Cooper, Phys. Rev. **137**, A1364 (1965).
[32] B. W. Shore, Phys. Rev. **171**, 43 (1968).
[33] M. J. Seaton, Rep. Prog. Phys. **46**, 167 (1983).
[34] L. Minnhagen, J. Opt. Soc. Am. **63**, 1185 (1973).
[35] J. Landais, M. Huet, H. Kucal, and T. Dohnalik, J. Phys. B **28**, 2395 (1995).
[36] I. Velchev, W. Hogervorst, and W. Ubachs, J. Phys. B **32**, L511 (1999).
[37] J. Bömmels, J. M. Weber, A. Gopalan, N. Herschbach, E. Leber, A. Schramm, K. Ueda, M.-W. Ruf, and H. Hotop, J. Phys. B **32**, 2399 (1999).
[38] C. Yamada, H. Kanamori, and E. Hirota, J. Chem. Phys. **83**, 552 (1985).
[39] F. DiFilippo, V. Natarajan, K. R. Boyce, and D. E. Pritchard, Phys. Rev. Lett. **73**, 1481 (1994).
[40] D. L. Farham, R. S. Van Dyck, Jr., and P. B. Schwinberg, Phys. Rev. Lett. **75**, 3598 (1995).
[41] Th. Udem, A. Huber, B. Gross, J. Reichert, M. Prevedelli, M. Weitz, and T. W. Hänsch, Phys. Rev. Lett. **79**, 2646 (1997).
[42] A. Muhlpfordt and U. Even, J. Chem. Phys. **103**, 4427 (1995).
[43] L. C. Lee, G. P. Smith, T. M. Miller, and P. C. Cosby, Phys. Rev. A **17**, 2005 (1978).
[44] J. T. Moseley, R. T. Saxon, B. A. Huber, P. C. Cosby, R. Abouaf, and M. Tadjeddine, J. Chem. Phys. **67**, 1659 (1977).